The Meteoritical Society

Meteoritics & Planetary Science 44, Nr 4, 505–519 (2009)
Abstract available online at http://meteoritics.org

An investigation of the behavior of Cu and Cr during iron meteorite crystallization

Nancy L. CHABOT[1*], Sarah A. SASLOW[2], William F. McDONOUGH[3], and John H. JONES[4]

[1]Applied Physics Laboratory, 11100 Johns Hopkins Road, Laurel, Maryland 20723, USA
[2]University of Maryland, College Park, Maryland 20742, USA
[3]Department of Geology, University of Maryland, College Park, Maryland 20742, USA
[4]NASA Johnson Space Center, Mailstop KR, Houston, Texas 77058, USA
[*]Corresponding author. E-mail address: Nancy.Chabot@jhuapl.edu

(Received 19 May 2008; revision accepted 14 December 2008)

Abstract–The measured Cu and Cr contents in magmatic iron meteorites appear to contradict the behavior predicted by experimental fractional crystallization studies currently available. To investigate the origin of Cu and Cr concentrations observed in these meteorites, a thorough set of solid metal/liquid metal experiments were conducted in the Fe-Ni-S system. In addition to Cu and Cr, partitioning values were also determined for As, Au, Bi, Co, Mo, Ni, Pb, Rh, Ru, Sb, Sn, V, and Zn from the experiments. Experimental results for Cu and Cr showed similar chalcophile partitioning behavior, whereas these elements have differently sloped trends within magmatic iron meteorite groups. Thus, fractional crystallization alone cannot control both the Cu and Cr concentrations in these iron meteorite groups. A simple fractional crystallization model based on our experimental Cu partitioning results was able to match the Cu versus Au trend observed in the S-poor IVB iron meteorite group but not the decreasing Cu versus Au trends in the IIAB and IIIAB groups or the unique S-shaped Cu versus Au trend in the IVA group. However, the crystallization model calculations were found to be very sensitive to the specific choice for the mathematical expression of D(Cu), suggesting that any future refinement of the parameterization of D(Cu) should include a reassessment of the Cu fractional crystallization trends. The Cr versus Au trends in magmatic iron meteorite groups are steeper than those of Cu and not explained by fractional crystallization. Other influences, such as the removal of chromite from the crystallizing system or sampling biases during iron meteorite compositional analyses, are likely responsible for the Cr trends in magmatic iron meteorite groups.

INTRODUCTION

Magmatic iron meteorites are believed to be samples of the metallic cores of asteroid-sized parent bodies. Element-element trends in iron meteorite groups suggest that iron meteorites evolved by fractional crystallization (Scott 1972). Modeling the crystallization of iron meteorites in detail has provided insights into the compositional evolution of asteroidal cores (e.g., review by Chabot and Haack 2006).

Early studies of iron meteorite crystallization (Scott 1972) concluded that elements with solid metal/liquid metal partition coefficients (D) > 1, such as Ir, decrease in concentration as fractional crystallization progresses in magmatic iron meteorite groups; since Ir prefers the solid metal to the liquid metal, as fractional crystallization proceeds, the amount of Ir that has not already partitioned into the solid metal decreases and, consequently, later crystallizing solids contain less Ir. Conversely, an element such as Au, with D < 1, has increased concentrations in later crystallizing solids. A plot of Ir versus Au for a fractionally crystallized magmatic iron meteorite group thus shows a negative trend.

However, detailed modeling studies of the crystallization of iron meteorites demonstrate that it is not just the value of D that influences the resulting crystallization trend but also how D changes as crystallization proceeds (e.g., Jones 1994). The concentration of S in the asteroidal core has a significant effect on how elements behave during core crystallization (e.g., Willis and Goldstein 1982; Jones and Drake 1983; Malvin et al. 1986). Initially, solid metal crystallizes from a completely molten core, but as crystallization proceeds, the concentration of S in the molten portion of the core increases, since S is excluded from the crystallizing solid metal. The

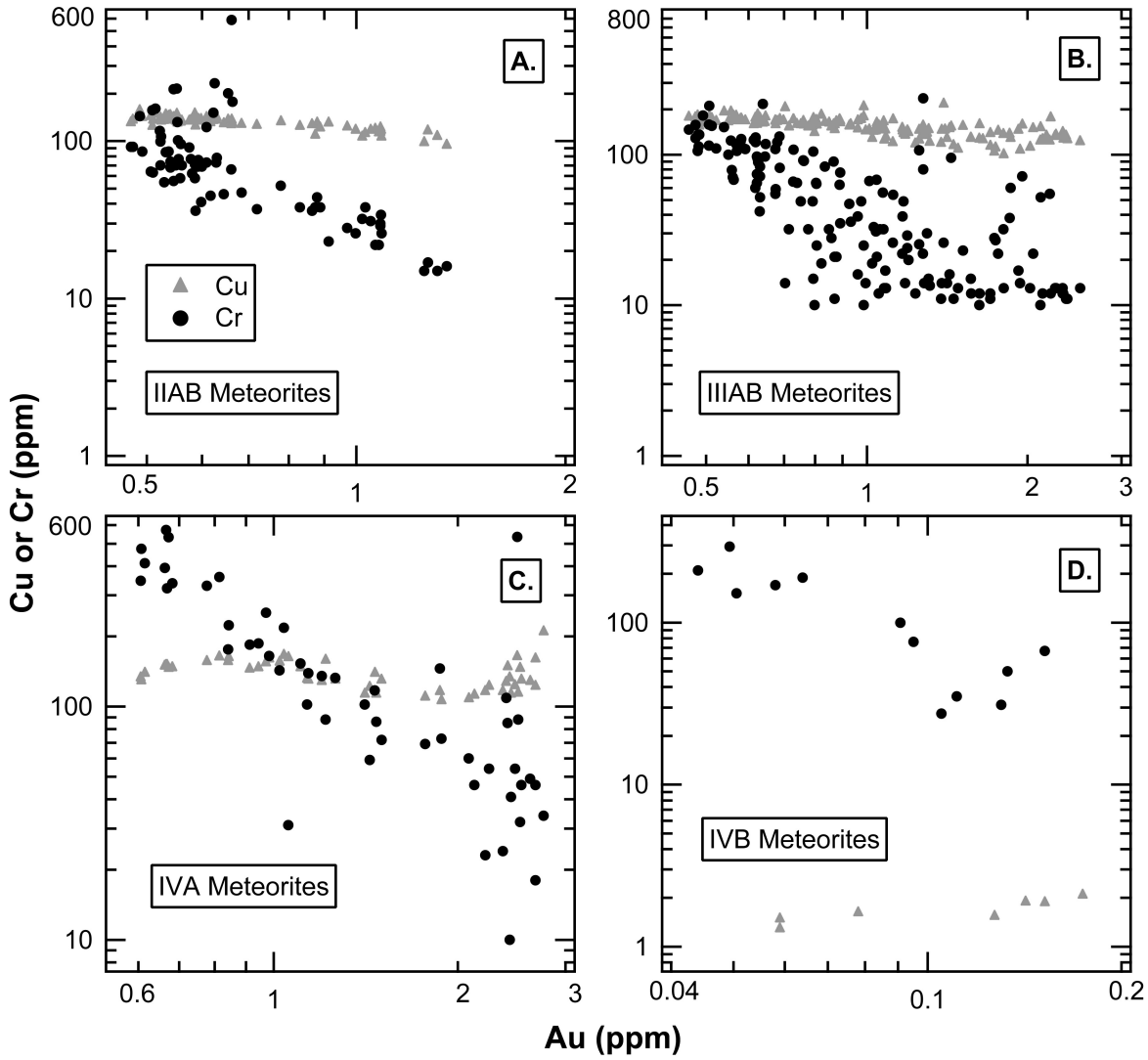

Fig. 1. The concentrations of Cu and Cr are plotted against Au for A) the IIAB, B) IIIAB, C) IVA, and D) IVB iron meteorite groups. The Cu and Cr trends are quite distinct from each other in each group. For the IIAB, IIIAB, and IVA groups, iron meteorite data were provided by J. T. Wasson and are largely from Wasson (1999), Wasson and Richardson (2001), and Wasson et al. (2007). For the IVB group, iron meteorite data are from Campbell and Humayun (2005) and Walker et al. (2008).

amount of S in the liquid can have a pronounced effect on the partition coefficients of elements. For example, D(Ga) and D(Ge) both increase with increasing S content of the metallic liquid, changing from incompatible to compatible in solid metal and resulting in the unique curved crystallization trends observed for these elements in many magmatic iron meteorite groups (e.g., Jones and Drake 1983; Haack and Scott 1993; Chabot 2004).

Modeling the crystallization of iron meteorite has largely focused on siderophile elements traditionally used for classification purposes: Au, Ga, Ge, Ir, and Ni (e.g., Jones and Drake 1983; Haack and Scott 1993; Ulff-Møller 1998; Wasson 1999; Wasson and Richardson 2001; Chabot 2004; Wasson et al. 2007). In the Fe-Ni-S system, these elements partition more strongly into the crystallizing solid metal as the S content of the metallic liquid increases. In contrast, Cu and Cr are chalcophile (S-loving) and partition more strongly into the liquid metal as its S content increases. Figure 1 shows Cu and Cr elemental trends versus Au for four magmatic iron meteorite groups, the IIIAB, IIAB, IVA, and IVB groups (Wasson 1999; Wasson and Richardson 2001; Campbell and Humayun 2005; Wasson et al. 2007; Walker et al. 2008). With the exception of Cu in the IVB group, Cu and Cr exhibit decreasing concentrations with increasing Au, though the Cr trends are considerably steeper than the Cu trends.

That either the Cu or the Cr versus Au trend decreases is an unexplained observation, since the available experimental data indicate that both D(Cu) and D(Cr) are <1 for these systems (Bild and Drake 1978; Chabot et al. 2003; Jones and Malvin 1990). One might thus expect that fractional

crystallization increases, not decreases, the amounts of Cr and Cu in the liquid metal as crystallization proceeds, similar to the trends observed for Au. However, detailed modeling of the crystallization process has not been investigated for these chalcophile elements, and, as shown for Ga and Ge, the changing partitioning behavior during crystallization can have a significant effect on the resulting elemental trends. The chalcophile behaviors of Cu and Cr may result in crystallization trends different than those for elements with siderophile behavior in the Fe-Ni-S solid metal-liquid metal system.

Additionally, the available partitioning data for D(Cr) and D(Cu) show similar solid metal/liquid metal behavior for both elements (Bild and Drake 1978; Jones and Malvin 1990; Chabot et al. 2003). In contrast, iron meteorite groups exhibit very different elemental trends for Cu and Cr, as shown in Fig. 1. This contradiction suggests that either the Cu and Cr trends cannot both be formed by fractional crystallization or that the current partitioning data are too limited to show the true behavior of Cr during iron meteorite crystallization. Experimental determinations of D(Cr) are restricted to five measurements, with S contents either below 5 wt% or above 28 wt% (Bild and Drake 1978; Jones and Malvin 1990; Chabot et al. 2003). No measurements of D(Cr) at intermediate S contents in the Fe-Ni-S system are available, and this compositional range is crucial for understanding the crystallization of iron meteorites.

To better understand the Cu and Cr trends observed in magmatic iron meteorite groups, and thus gain insight into the processes operating during the crystallization of asteroidal cores, we undertook an experimental study to determine the solid metal/liquid partitioning behavior of Cu and Cr in the Fe-Ni-S system. Experimental results reported here were then used to model iron meteorite crystallization.

EXPERIMENTAL PROCEDURES

Experiments were conducted at 1 atm in a Deltech vertical tube furnace at the Johns Hopkins University Applied Physics Laboratory, using methods similar to previous solid metal/liquid metal partitioning studies (e.g., Jones and Drake 1983; Chabot et al. 2007). Starting powders of commercially purchased pure Fe, FeS, and Ni were mixed to create a range of starting S concentrations. Nickel was added at about a 10 wt% level. In the experiments, Cr was designed to be a trace element and added at a level of about 0.5 wt%. Previous experimental studies that added Cr at lower levels of around 100 ppm discovered that Cr was often lost from the experimental sample, possibly into the alumina crucible used in the experiments (e.g., Chabot et al. 2003). Also, Cr is heterogeneously distributed in many of the iron meteorite samples used for analysis standards, complicating the analysis of Cr when it is present at low levels. Thus, since Cr is a major focus of our study, we decided to dope Cr at a level which the analysis could be conducted using the electron microprobe and which our prior experience indicated that such experiments would be successful (Hongsresawat et al. 2001).

Our other trace element of focus for this study was Cu, which we doped at a level of about 100 ppm. At this low level, it is possible to include multiple trace elements in the study with little additional effort and without affecting the partitioning behaviors (e.g., Chabot et al. 2003, 2007). Consequently, we reviewed the available experimental solid metal/liquid metal partitioning data in the Fe-Ni-S system and decided to also include As, Au, Bi, Co, Mo, Pb, Rh, Ru, Sb, Sn, V, and Zn. Each of these elements was added to the starting mixtures at a level of about 100 ppm.

About 200 mg of the starting powders were placed into pure silica tubes. Alumina crucibles were not used to hold the powders, as Chabot et al. (2007) demonstrated that the use of alumina crucibles was not necessary for solid metal/liquid metal partitioning experiments in the Fe-Ni-S system. The silica tubes were evacuated and hung in the furnace. Run temperatures ranged from 1050 °C to 1450 °C, and the duration of the run was inversely proportional to the temperature, ranging from 1 week to 16 hours. At a temperature of 1250 °C, Malvin et al. (1986) conducted a time series and demonstrated that similar trace element partitioning behavior was achieved for experiments that were conducted for 21 days to just 5 hours. We conducted a series of experiments with varying durations at 1050 °C, and experiments run for 72 h or less exhibited noticeably large Ni compositional variations within the normally homogenous solid metal. Additionally, measured D(Ni) values for these experiments were not in agreement with the numerous previous solid metal/liquid metal determinations of D(Ni) (references given in Appendix A). This suggests that a duration of longer than 72 h is needed to reach equilibrium when conducting solid metal/liquid metal experiments in the Fe-Ni-S system at 1 atm and 1050 °C using the methods employed in this study.

When each experiment was completed, the tube was removed from the furnace and briefly immersed in cold water, quenching the experimental sample. The sample, a shiny metallic bead, was mounted in epoxy and sliced using a diamond saw. A cross section of the sample was polished using alumina powder. Table 1 gives details about the run conditions of the seven individual experiments.

ANALYTICAL METHODS

Experiments were first inspected using the JEOL 8900L electron microprobe at the Carnegie Institution of Washington. Figure 2 shows a backscattered electron (BSE) image of run #IT14, which illustrates the typical textures present in each experiment. The solid metal and liquid metal were clearly separated in the experimental run products, and

Table 1. Experimental run conditions, compositions, and partition coefficients.

Run #	IT10	IT11	IT14	IT3	IT4	IT5	IT9
T (°C)	1450	1400	1375	1350	1300	1250	1050
Duration (h)	16	23	74	17	24	15	168
Liquid metal							
Fe (wt%)	83.9 ± 0.8	79.2 ± 1.0	76.6 ± 0.5	70.3 ± 1.0	65.2 ± 1.4	63.1 ± 1.2	60.5 ± 1.1
Ni (wt%)	11.6 ± 0.2	11.2 ± 0.2	9.20 ± 0.13	9.0 ± 0.3	8.9 ± 0.5	9.2 ± 0.6	6.9 ± 0.8
S (wt%)	3.4 ± 0.4	8.2 ± 1.0	12.8 ± 0.5	19.7 ± 1.2	24 ± 2	26 ± 2	30.5 ± 1.1
Cr (wt%)	0.6 ± 0.1	0.71 ± 0.09	1.11 ± 0.06	0.57 ± 0.04	0.9 ± 0.1	0.66 ± 0.08	0.52 ± 0.08
As (ppm)	6.3 ± 0.7	6.1 ± 0.7	3.60 ± 0.05	5 ± 1	3.6 ± 0.5	4 ± 1	2.5 ± 1.2
Au (ppm)	220 ± 40	240 ± 30	110 ± 8	47 ± 9	110 ± 20	51 ± 4	30 ± 20
Bi (ppm)	900 ± 100	–	960 ± 80	300 ± 70	1000 ± 300	400 ± 100	300 ± 100
Co (ppm)	110 ± 11	81.5 ± 0.9	42 ± 2	47 ± 4	42 ± 2	44 ± 4	34 ± 6
Cu (ppm)	330 ± 50	400 ± 20	760 ± 40	370 ± 20	800 ±100	490 ± 60	500 ± 100
Mo (ppm)	130 ± 30	130 ± 9	160 ± 3	69 ± 8	160 ± 20	130 ± 30	100 ± 20
Pb (ppm)	1300 ± 200	–	1000 ±100	–	1000 ± 300	500 ±100	600 ± 300
Rh (ppm)	69 ± 12	38 ± 5	16 ± 3	–	16 ± 2	–	–
Ru (ppm)	67 ± 14	28 ± 7	8 ± 3	–	8.0 ± 1.4	–	–
Sb (ppm)	460 ± 80	310 ± 20	380 ± 50	170 ± 20	400 ± 200	190 ± 70	140 ± 40
Sn (ppm)	390 ± 70	240 ± 30	290 ± 40	140 ±11	300 ± 100	130 ± 40	100 ± 30
V (ppm)	140 ± 40	200 ± 30	380 ± 7	130 ± 20	380 ± 40	160 ± 10	60 ± 10
Zn (ppm)	270 ± 40	370 ± 40	490 ± 40	140 ± 20	490 ± 60	320 ± 30	50 ± 13
Solid metal							
Fe (wt%)	88.7 ± 0.12	88.6 ± 0.2	89.7 ± 0.2	88.7 ± 0.4	87.7± 0.4	86.5 ± 0.2	86.2 ± 0.6
Ni (wt%)	10.9 ± 0.2	10.7 ± 0.1	9.44 ± 0.02	10.23 ± 0.14	11.68 ± 0.12	12.80 ± 0.14	13.03 ± 0.12
Cr (wt%)	0.46 ± 0.03	0.49 ± 0.03	0.51 ± 0.01	0.15 ± 0.03	0.17 ± 0.04	0.13 ± 0.04	0.08 ± 0.03
As (ppm)	–	2.1 ± 0.7	1.9 ± 0.5	3.3 ± 0.9	5.0 ± 0.5	7.3 ± 1.4	17.1 ± 1.3
Au (ppm)	64 ± 4	89 ± 8	82 ± 2	50 ± 2	190 ± 50	180 ± 50	210 ± 4
Bi (ppm)	1.8 ± 0.3	–	0.41 ± 0.07	0.11 ± 0.02	–	–	–
Co (ppm)	140 ± 6	130 ± 3	115.5 ± 1.2	140 ± 4	150 ± 5	170 ± 9	180 ± 3
Cu (ppm)	140 ± 20	130 ± 4	160 ± 5	110 ± 20	180 ± 13	120 ± 20	94.7 ± 1.3
Mo (ppm)	110 ± 20	110 ± 5	130 ± 5	140 ± 6	490 ± 70	340 ± 70	310 ± 13
Pb (ppm)	5.7 ± 0.5	–	1.72 ± 0.12	–	–	–	0.26 ± 0.04
Rh (ppm)	120 ± 12	110 ± 4	150 ± 2	–	400 ± 30	–	–
Ru (ppm)	150 ± 14	130 ± 3	190 ± 3	–	450 ± 80	–	–
Sb (ppm)	30 ± 5	20 ± 6	26 ± 1.2	17.6 ± 0.6	60 ± 4	40 ± 10	78 ± 3
Sn (ppm)	30 ± 4	21 ± 6	28 ± 2	26 ± 3	88 ± 5	60 ± 10	99 ± 6
V (ppm)	28 ± 2	23.3 ± 1.1	27.7 ± 0.5	8.2 ± 0.8	17.7 ± 0.6	5.7 ± 1.0	0.69 ± 0.07
Zn (ppm)	83 ±12	100 ± 20	93 ± 6	34 ± 7	150 ± 30	80 ± 30	14.50 ± 0.01
Partition coefficients							
D(As)	–	0.34 ± 0.11	0.35 ± 0.09	0.7 ± 0.2	1.4 ± 0.2	1.9 ± 0.6	4 ± 3
D(Au)	0.29 ± 0.05	0.38 ± 0.06	0.53 ± 0.04	1.1 ± 0.2	1.8 ± 0.6	3.6 ± 1.0	8 ± 5
D(Bi)	0.0021 ± 0.0004	–	0.00045 ± 0.00008	0.00037 ± 0.0001	–	–	–
D(Co)	1.26 ± 0.13	1.58 ± 0.04	2.0 ± 0.1	2.0 ± 0.3	3.7 ± 0.2	3.9 ± 0.4	5.5 ± 1.0
D(Cr)	0.7 ± 0.1	0.67 ± 0.09	0.46 ± 0.03	0.26 ± 0.06	0.20 ± 0.05	0.20 ± 0.07	0.16 ± 0.06
D(Cu)	0.43 ± 0.08	0.32 ± 0.02	0.33 ± 0.02	0.33 ± 0.05	0.24 ± 0.05	0.24 ± 0.04	0.18 ± 0.04
D(Mo)	0.8 ± 0.2	0.86 ± 0.07	1.23 ± 0.05	1.2 ± 0.3	3.1 ± 0.6	2.7 ± 0.8	3.1 ± 0.5
D(Ni)	0.94 ± 0.05	0.96 ± 0.04	1.02 ± 0.03	1.1 ± 0.1	1.3 ± 0.2	1.4 ± 0.2	1.9 ± 0.5
D(Pb)	0.0045 ± 0.0009	–	0.0014 ± 0.0002	–	–	–	0.0005 ± 0.0002
D(Rh)	1.7 ± 0.3	2.8 ± 0.4	4.2 ± 0.7	–	26 ± 3	–	–
D(Ru)	2.3 ± 0.5	4.6 ± 1.2	7.1 ± 2.3	–	57 ± 14	–	–
D(Sb)	0.06 ± 0.02	0.07 ± 0.02	0.065 ± 0.009	0.07 ± 0.01	0.15 ± 0.06	0.22 ± 0.09	0.6 ± 0.2
D(Sn)	0.08 ± 0.02	0.09 ± 0.03	0.102 ± 0.013	0.10 ± 0.03	0.30 ± 0.11	0.4 ± 0.2	1.0 ± 0.3
D(V)	0.20 ± 0.06	0.12 ± 0.02	0.103 ± 0.003	0.10 ± 0.01	0.046 ± 0.005	0.035 ± 0.006	0.011 ± 0.002
D(Zn)	0.30 ± 0.06	0.28 ± 0.05	0.26 ± 0.03	0.26 ± 0.06	0.29 ± 0.07	0.2 ± 0.1	0.28 ± 0.07

Data for Fe, Ni, S, and Cr are from electron microprobe analysis. All other data are from laser ablation ICP-MS microanalysis.
Errors are ±2σ.

the solid metal was homogenous. The liquid metal was a single phase at the run conditions, but upon quenching formed a dendritic texture of Fe-Ni dendrites surrounded by interstitial S-rich material.

Concentrations of the major elements of Fe, Ni, and S and the minor element of Cr were determined using the electron microprobe. Beam conditions of 15 kV and 30 nA were used for all analysis with 30 second counting times. Measurements were made using a defocused beam with a diameter of 20 μm, with multiple measurement points collected in each phase. For the solid metal, 11–15 measurements were collected for each experiment and showed the solid metal to be homogenous. For the liquid metal, 25–30 analysis points were averaged together to determine the bulk composition of the quenched metallic liquid. Using image processing and analysis techniques, Chabot and Drake (1997) demonstrated that this analysis approach produces reliable bulk compositions for Fe-S liquids with similar dendritic quench textures. Errors for each phase were calculated as twice the standard error of the mean of the multiple analyses. Table 1 provides the measured concentrations for the major elements and Cr as determined by electron microprobe analysis.

Trace element concentrations were determined by laser ablation inductively coupled plasma mass spectrometry (ICP-MS) microanalysis at the University of Maryland. Analyses were conducted using a single-collector ICP-MS (Element 2, Thermo Electron Corp) coupled to a laser ablation system with an output wavelength at 213 nm (UP213, New Wave Research). The laser was operated at 2.4 J/cm^2. Ablation sampling was done in line scan mode using a 30 μm diameter spot and 7 Hz flash rate for the solid metal and a 80 μm diameter spot and 5 Hz flash rate for the liquid metal. During ablation, the sample was moved at a rate of 10 μm/s. The length of each line varied depending on the characteristics of each experimental sample, but the length was generally between 300 to 1000 μm. Four line scans were conducted in each solid metal and liquid metal phase. This analysis approach has been proven to be effective for measuring the compositions of similar experimental samples with solid metal and liquid metal present (Chabot et al. 2003, 2007).

During analysis, data were collected for the following masses: ^{51}V, ^{53}Cr, ^{57}Fe, ^{59}Co, ^{62}Ni, ^{63}Cu, ^{65}Cu, ^{66}Zn, ^{67}Zn, ^{75}As, ^{95}Mo, ^{97}Mo, ^{99}Ru, ^{101}Ru, ^{103}Rh, ^{117}Sn, ^{118}Sn, ^{121}Sb, ^{123}Sb, ^{197}Au, ^{206}Pb, ^{208}Pb, and ^{209}Bi. Analyses of two standard reference materials (NIST 610 and Filomena) were conducted both before and after the analyses of the experimental run products, which provided the basis for determining calibration curves to constrain instrument drift and provide element concentrations. Data were processed using the LAMTRACE (Achterbergh et al. 2001) software program, which determines element concentrations using ratios of count rates for samples and standards, known concentrations in the standards, and the known concentration of an internal standard in the experimental run products. Errors in the composition of each phase were calculated as twice the standard error of the mean, and the measurements are reported in Table 1. Measurements below the detection limit, defined as background plus three standard deviations of the background, or measurements where the standard error of the mean was greater than 33% are not reported in Table 1.

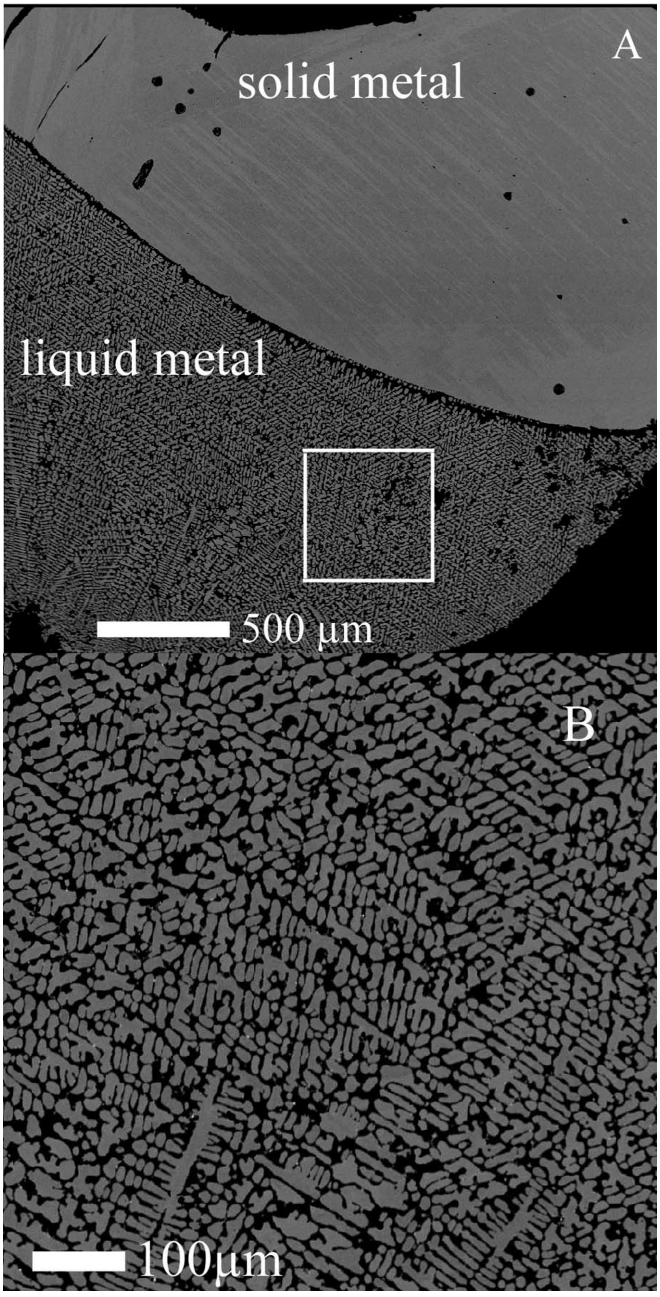

Fig. 2. A. The experiment #IT14 is shown in a backscattered electron image. The Fe-Ni solid metal was homogenous but the S-bearing metallic liquid quenched to a dendritic texture. B. A close-up of a portion of the metallic liquid shows the metallic liquid quench texture is composed of Fe-Ni dendrites and S-rich interstitial material.

PARTITIONING RESULTS

The calculated solid metal/liquid metal weight ratio partition coefficient, D, for each element in each experiment is given in Table 1. Errors in D are propagated from the errors in the solid metal and liquid metal phases, assuming independent errors in the solid and liquid concentration measurements. Figure 3 plots the partitioning results for 10 of the trace elements in our experiments as a function of the S content of the metallic liquid. Our new partitioning results are in good agreement with the available previous determinations, the references for which are detailed in Appendix A (Bild and Drake 1978; Willis and Goldstein 1982; Jones and Drake 1983; Jones and Malvin 1990; Fleet and Stone 1991; Lodders and Palme 1991; Jones et al. 1993; Fleet et al. 1999; Liu and Fleet 2001; Chabot et al. 2003; Appendix B).

Typical siderophile behavior in the Fe-Ni-S system is exhibit by As, Au, Co, Mo, Ni, Rh, Ru, Sb, and Sn, with these elements partitioning more strongly into the solid metal as the S content of the metallic liquid increases. For the Fe-Ni-S system, the Chabot and Jones (2003) parameterization has the form of:

$$\frac{1}{D} = \frac{(\text{Fe domains})^{\beta}}{D_O} \quad (1)$$

$$(\text{Fe domains}) = \frac{(1 - 2X_S)}{(1 - X_S)} \quad (2)$$

with β and D_O as constants unique to the element parameterized and "Fe domains" is established by the fraction of free Fe in the liquid metal, assuming the speciation in the liquid metal is a combination of free Fe and FeS. X_S is the molar concentration of S in the metallic liquid. Sufficient data existed for Chabot and Jones (2003) to parameterize D(As), D(Au), D(Co), and D(Ni). Combining both our new data and data from previous studies results in only insignificant changes to the parameterized fits of D(As), D(Au), and D(Co) and no change in the fit of D(Ni), as shown in Fig. 3. For Mo, Rh, Ru, Sb, and Sn, we provide parameterized fits for the first time for the solid metal/liquid metal partitioning behavior of these elements using the form of Chabot and Jones (2003). These fits are shown on Fig. 3, and Table 2 lists the values of D_O and β.

The solid metal/liquid metal partitioning behavior of Zn is noticeably different from the other elements plotted in that Fig. 3. Over the large range of S contents covered in our experiments, D(Zn) stays essentially constant at a value of about 0.3. No other element exhibits a constant solid metal/liquid metal partitioning behavior in the Fe-Ni-S system despite varying metallic liquid S concentrations. Some elements, such as Ni, exhibit essentially constant solid metal/liquid partitioning behavior in the Fe-Ni-P system (e.g., Corrigan et al. 2009), but Zn is the first element observed to behave this way in the Fe-Ni-S system. A constant partition coefficient despite changing metallic liquid S concentrations would suggest that Zn equally prefers partitioning into both the free Fe and FeS domains and balances out these competing siderophile and chalcophile tendencies.

Figure 4 shows the partitioning results for the five elements that exhibited chalcophile behavior in our experiments: Bi, Pb, Cr, Cu, and V. Our results for Cu and Cr are in good agreement with determinations from previous experimental studies, which are detailed in Appendix A (Bild and Drake 1978; Jones and Malvin 1990; Chabot et al. 2003; Appendix B). Our results are also consistent with the chalcophile behaviors observed for both Bi and Pb in the Ni-S system and in high Ni experiments in the Fe-Ni-S system (Chabot et al. 2007). In addition, metal/silicate partitioning experiments with V and Cr showed chalcophile behavior for both of these elements (Chabot and Agee 2003), just as observed in our experiments.

However, our results show very similar values for D(Cu) and D(Cr) over the entire range of S contents investigated. Thus, any fractional crystallization model based on the solid metal/liquid metal partitioning behaviors of Cu and Cr in the Fe-Ni-S system would produce similar crystallization trends for these two elements. In contrast, the magmatic iron meteorite groups plotted in Fig. 1 clearly show significantly different elemental trends for Cu and Cr within each iron meteorite group. In the next section, we investigate the elemental trends produced by the fractional crystallization of a chalcophile element, specifically Cu. However, even without detailed modeling, our partitioning results clearly indicate that the trends of Cu and Cr cannot both be explained by just fractional crystallization.

MODELING IRON METEORITE CRYSTALLIZATION

Modeling Method

All fractional crystallization model calculations were carried out using the approach detailed in Chabot (2004). Simple fractional crystallization is treated as the crystallization of solid metal in small increments, with the solid being removed from the crystallizing system after each single step increment. After each crystallization increment, the remaining liquid has a slightly altered composition from the bulk composition. This slightly altered liquid then becomes the initial bulk composition for the next incremental crystallization step. The model calculations only involve the most basic, simple fractional crystallization calculations, which are fundamentally based on mass balance equations, applied to each single step crystallization increment:

$$C_L = \frac{C_i}{(1 - f + fD)} \quad (3)$$

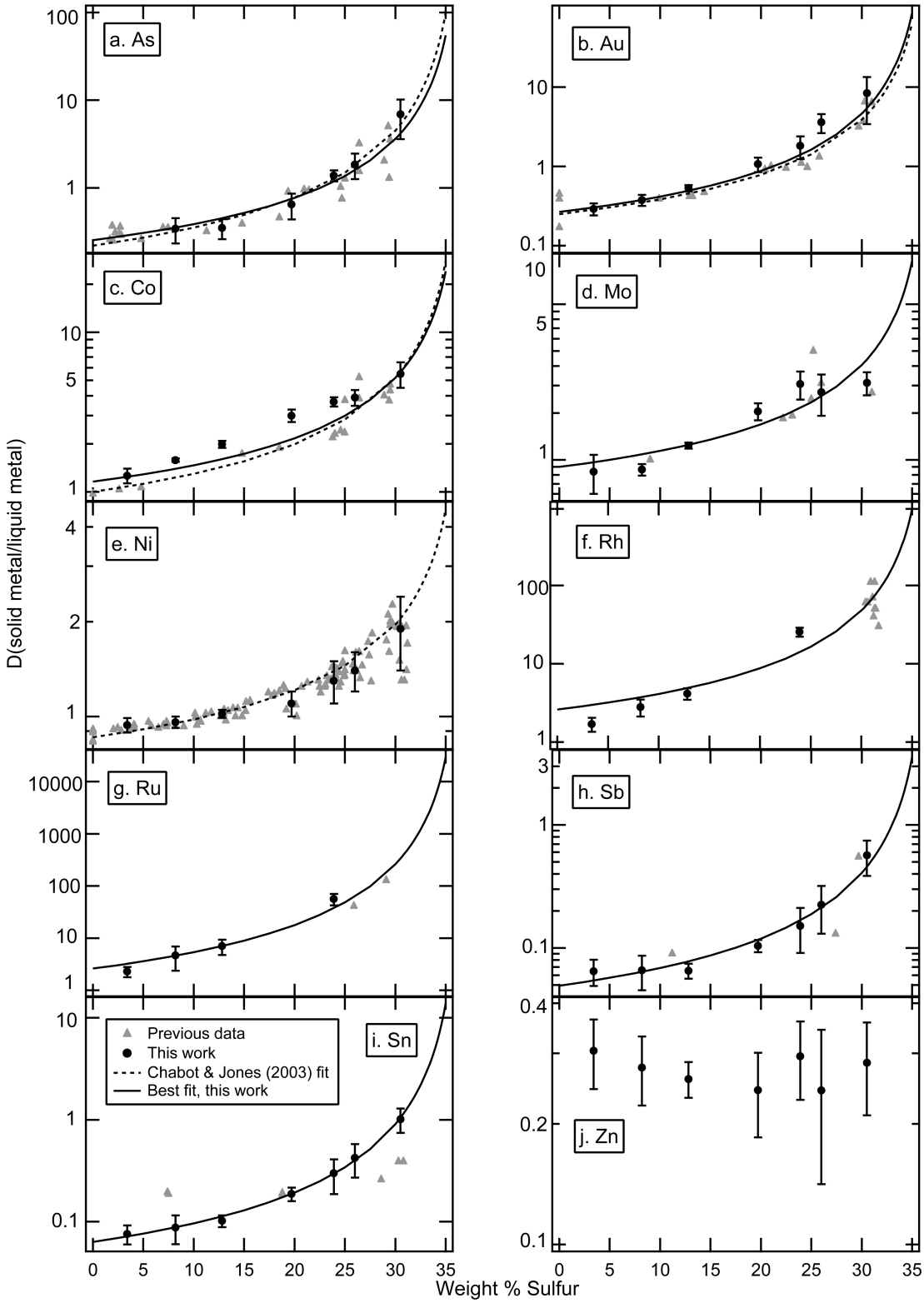

Fig. 3. Experimental solid metal/liquid metal partitioning results are shown for elements that exhibit siderophile behavior, with increasing D values as the S content of the metallic liquid increases. These elements include: a) As, b) Au, c) Co, d) Mo, e) Ni, f) Rh, g) Ru, h) Sb, and i) Sn. Experimental results are also shown for (j). Zn, which shows no change in its partition coefficient with changing S content of the metallic liquid. References for the previous experimental data are given in Appendix A. The parameterization values for the fits to the data are given in Table 2.

Table 2. Values for fitted parameterizations.

Element	D_0 (wt%)	β
As	0.25	1.9
Au	0.27	2.1
Co	1.2	1.1
Mo	0.9	1.1
Rh	2.6	2.1
Ru	2.6	3.4
Sb	0.05	1.5
Sn	0.10	1.1

$$C_S = D(C_L) \quad (4)$$

C_i is the bulk composition of the liquid prior to crystallization, f is the fraction of solid metal that crystallizes during each single step, D is the solid metal/liquid metal partition coefficient, and C_S and C_L are the compositions of the crystallizing solid and the residual liquid respectively for each step. The parameter of f is set to a value of 1/10,000 in our modeling work.

As crystallization proceeds, S is excluded from the solid metal and, consequently, the S content of the remaining metallic liquid increases. A D(S) value of 0.01 was used for crystallization calculations until a liquid S content of 31 wt% was reached, corresponding to the Fe-FeS eutectic. During each crystallization step, D values were calculated based on the S content of the liquid during that increment.

For our modeling efforts, we focused on the Cu versus Au crystallization trends; the behavior of Cr versus Au will follow similar trends based on the experimental data reported here (Fig. 4). Chemical variation trends with Au have been used because Au offers a larger dynamic range than Ni within iron meteorite groups and can be measured with good precision (Haack and Scott 1993; Wasson et al. 1998; Wasson 1999). For D(Au), Equation 1 was used along with the values for β and D_O given in Table 2.

For D(Cu), the functional form of the dependence on S is expected to be different than that of D(Au), due to the chalcophile nature of Cu. The Chabot and Jones (2003) parameterization model is appropriate for capturing the behavior of elements with siderophile behavior in the solid metal-liquid metal system, since D values reflect the functional availability of Fe domains. Chabot and Jones (2003) suggested that just as the partition coefficients for siderophile elements are functions of the Fe domains in the metallic liquid, the behavior of chalcophile elements should reflect the availability of FeS domains in the liquid. The fraction of Fe domains and fraction of FeS domains must add up to one in the Fe-S system, and the fraction of FeS domains is calculated as:

$$(\text{FeS domains}) = \frac{X_S}{(1 - X_S)} \quad (5)$$

X_S is the molar concentration of S in the metallic liquid. Using a form similar to that of Equation 1, but for FeS domains rather than Fe domains, leads to the following Equation 6:

$$\frac{1}{D} = \frac{(\text{FeS domains})^{\beta}}{D_S} \quad (6)$$

D is the solid metal/liquid metal partition coefficient, and D_S is the partition coefficient between solid metal and liquid metal with a liquid composition of FeS, about 36 wt% S. For Cu, using Equation 6, a best fit is given as:

$$\frac{1}{D(Cu)} = \frac{(\text{FeS domains})^{0.41}}{0.16} \quad (7)$$

The values of 0.41 and 0.16 were determined by expressing Equation 6 as ln(D) and determining the best linear fit. Figure 5a shows the fit from Equation 7 to the experimental D(Cu) data. The parameterization based as a function of the FeS domains predicts a steep dependence of D(Cu) on the S content at lower S levels and predicts D(Cu) changes less as the S content increases, a form that is consistent with the experimental D(Cu) data.

Jones and Malvin (1990) alternatively suggested that chalcophile elements follow an Fe domains fit, but that the β constant has an opposite sign. Using Equation 1, D(Cu) was also expressed as a best-fit function of Fe domains with a β value of –0.97 and a D_O value of 0.51; the values of –0.97 and 0.51 were calculated based on the best linear fit to expressing Equation 1 as ln(D). This Fe domains based fit is also shown on Fig. 5a and produces a curve that is fairly level at low S contents and changes steeply at higher S contents, opposite to the fit based on FeS domains and inconsistent with the experimental data shown on Fig. 5a.

In actuality, the value of D(Cu) must be influenced by both Fe and FeS domains (Chabot and Jones 2003). Equation 6 breaks down in the S-free system, when FeS domains equal zero, and consequently D would be calculated to be infinite. Of course, D(Cu) in the S-free system is not infinite but rather has a value of about 0.6, as seen in Fig. 4d. Therefore, Equation 7, which is based solely on FeS domains, is not valid in the S-free system, and the influence of Fe domains on the behavior of D(Cu) must then be taken into account to get a meaningful determination of the partition coefficient at low S contents. However, as the S content of the metallic liquid increases, the influence of the FeS domains appears to dominate the effect of the Fe domains on the partitioning behavior of Cu. This statement is supported fundamentally by the observed chalcophile behavior of Cu and secondly by the relative success and failure of the FeS and Fe domains based fits respectively to match the functional dependence of D(Cu) on the S content of the metallic liquid in Fig. 5a. For our needs, we will model the fractional crystallization of Cu for systems that contain S. As seen on Fig. 5a, the FeS domains fit given in Equation 7 is consistent with the D(Cu) experimental data for S contents ≥3 wt%, and hence we will only use it for modeling systems with ≥3 wt% S.

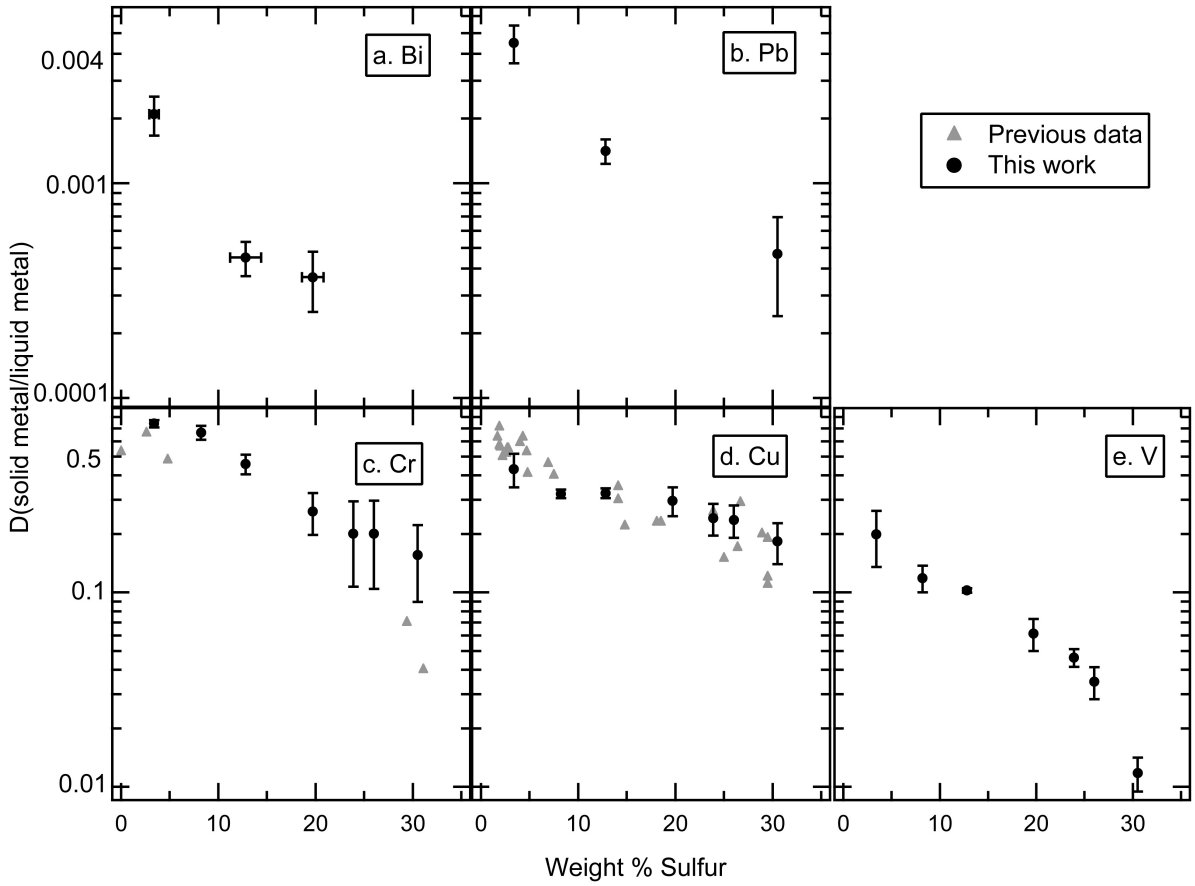

Fig. 4. Partitioning results are plotted for the five elements with chalcophile behavior in the experiments. These elements exhibit decreasing solid metal/liquid metal partitioning values with increasing S content of the metallic liquid: a) Bi, b) Pb, c) Cr, d) Cu, and e) V. References for the previous data are given in Appendix A.

Modeling Cu in Iron Meteorite Groups

A simple fractional crystallization model using the FeS domains-based fit for D(Cu) in Equation 7 was used for four different initial S contents, from 3 to 18 wt% S. The resulting solid metal Cu versus Au trends produced are very similar, regardless of initial S content (Fig. 5b). In Fig. 5b, the first solid metal produced in each model run was normalized to a composition of unity for Au and Cu; this choice enabled easy comparisons between the model runs with different initial S contents. The paths of the evolving liquid metal are also plotted on Fig. 5b and show more variation with varying S contents than the solid metal paths. The lack of variation in the shape of the solid metal paths is in striking contrast to the behavior of many other elements previously modeled in iron meteorites, such as Ga, Ge, and Ir, whose crystallization trends are very sensitive to the choice of the initial S content of the parent metallic melt (e.g., Jones and Drake 1983; Haack and Scott 1993; Ulff-Møller 1998; Wasson 1999; Chabot 2004).

Next, we applied our modeling results to four magmatic iron meteorite groups, as shown in Fig. 5c–f. Though x and y axes values are different for different iron meteorite groups, the range of each graph was purposely kept the same, aiding comparisons. Specifically, Fig. 5b–f all exhibit a factor of 10 on the x-axis and a factor of 20 on the y-axis.

The Cu versus Au trend for IVB irons, known to be a S-poor group, is consistent with an initial primary melt value of ~3 wt% S, as plotted in Fig. 5c. A value of 3 wt% S in the metallic liquid phase is the lowest S content we investigated, due to limitations of Equation 7 for the parameterization of D(Cu). A lower S content may also be consistent with the IVB Cu versus Au trend. The IVB meteorite data plotted on Fig. 5c are from Campbell and Humayun (2005). The recent Walker et al. (2008) study also reports Cu measurements in IVB irons, but as discussed in the electronic supplement to that work, Cu was observed to exhibit some heterogeneities on the scale of the analysis in that study. The scatter in the Walker et al. (2008) Cu measurements thus complicates the identification of the general IVB Cu crystallization trend, and we have consequently chosen to use only the Campbell and Humayun (2005) IVB data for our modeling purposes. Based on modeling highly siderophile element crystallization trends in the IVB group, Walker et al. (2008) suggested an initial S

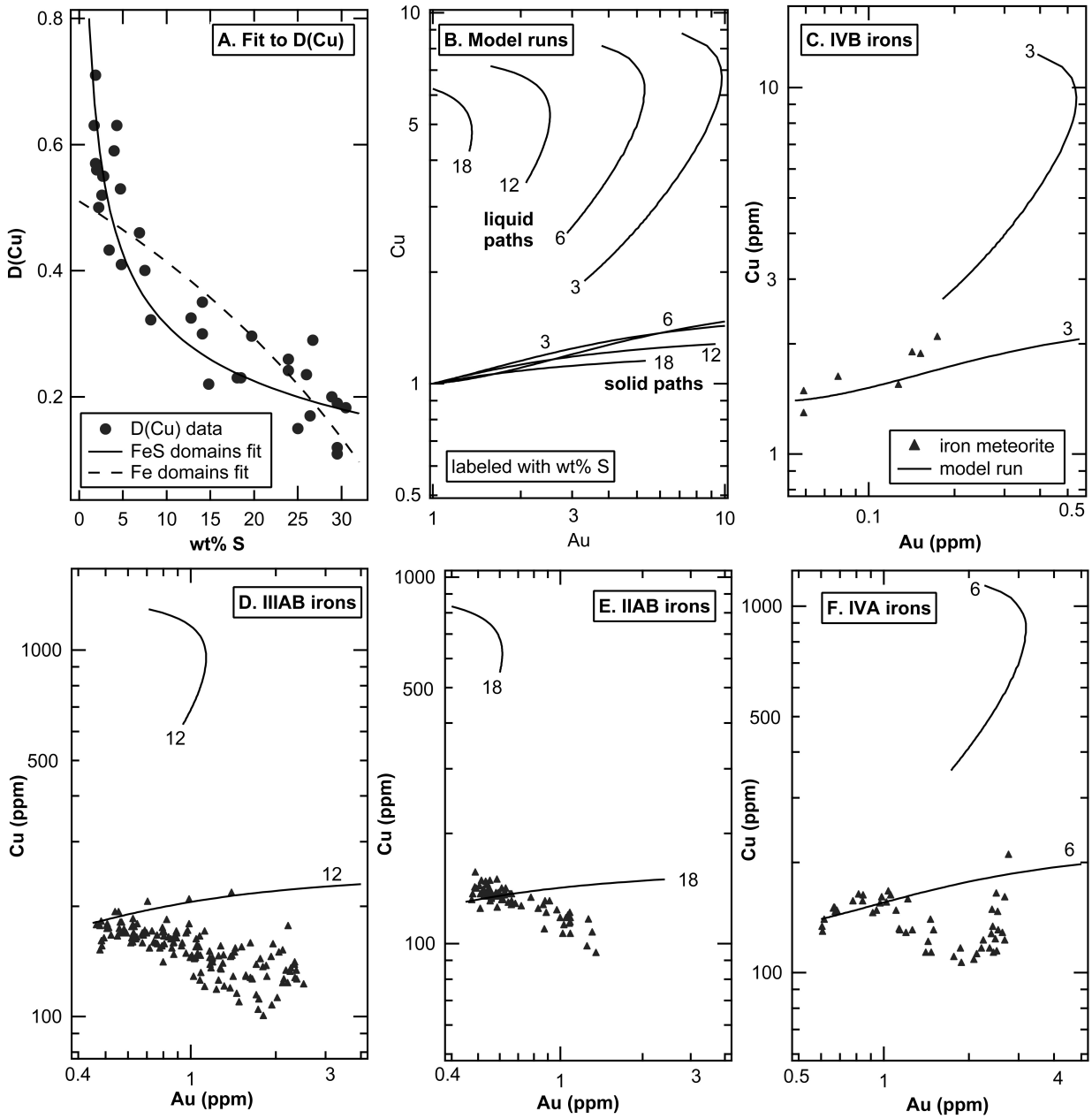

Fig. 5. Simple fractional crystallization modeling results are shown using a FeS domains based fit to the D(Cu) data. A) The FeS domains based fit used to express D(Cu) as a function of the wt% S in the metallic liquid is shown. B) Model results for different initial S contents are plotted, each normalized to have the first solid formed have values of one for both Cu and Au. Lines are labeled with the initial S content of each model calculation, and both solid and liquid crystallization paths are shown. Model runs are compared to Cu versus Au trends observed in C) the IVB, D) IIIAB, E) IIAB, and F) IVA iron meteorite groups. Graphs B–F are all shown on log scales with a factor of 10 on the x-axis and a factor of 20 on the y-axis for easy comparison. Iron meteorite data for the IIAB, IIIAB, and IVA groups was provided by J. T. Wasson and comes largely from Wasson (1999), Wasson and Richardson (2001), and Wasson et al. (2007). IVB meteorite data are from Campbell and Humayun (2005).

content for the IVB group of 0–2 wt%, with a preference for a value closer to 2 wt% than 0 wt%.

The Cu contents for the IIIAB (Wasson 1999) and IIAB groups (Wasson et al. 2007), in contrast to the IVB irons, decrease with increasing Au concentrations, as shown in Figs. 5d and 5e. None of our crystallization models (Fig. 5b) produce decreasing Cu versus Au trends, and thus the simple fractional crystallization model cannot explain the Cu trends in these two large magmatic iron meteorite groups. Using the same simple fractional crystallization model, Chabot (2004) determined S contents for the IIIAB and IIAB groups of 12 and 17 wt% S, respectively, based on fitting Ga, Ge, and Ir

versus Au trends in these groups. For the IIIAB group in Fig. 5d, the Cu versus Au model crystallization trend is shown for an initial S content of 12 wt%; the IIIAB irons show scatter in the Cu versus Au trend, but the simple fractional crystallization model is inconsistent with the IIIAB data. Similarly, a high S content, 18 wt% S, simple fractional crystallization model does not match the IIAB Cu versus Au trend on Fig. 5e.

A distinctive S-shaped Cu versus Au trend is observed for the IVA irons (Fig. 5f). By all measures, this unique S-shaped trend appears to be genuine, with replicate analyses reproducing the trend (Wasson and Richardson 2001). Additionally, graphing only IVA meteorites for which Cu data are available results in well-sampled and continuous IVA Ir versus Au and Ge versus Au trends, supporting the statement that the Cu versus Au S-shaped trend is not produced by a sampling artifact. Our crystallization models do not produce trends consistent with this S-shape. The IVA Cu trend is a unique chemical signature of the history of the IVA parent body. Chabot (2004) was unable to match the IVA trends of Ga, Ge, and Ir versus Au with a single S content, and no S content produced crystallization trends that were consistent with the highest-Au, latest crystallizing IVA irons. These high-Au IVA irons are the same ones that show increasing Cu contents, forming the second upward turn of the S-shaped trend in Fig. 5f. To date, no single crystallization model has adequately matched the Ga, Ge, and Ir contents of the high-Au IVA irons. Based on modeling Ga, Ge, and Ir versus Au, Chabot (2004) suggested that the IVA initial S content was between 3–9 wt% S. As shown on Fig. 5f, an initial S content of 6 wt% S does not produce a Cu versus Au trend consistent with the IVA meteorite data.

Overall, simple fractional crystallization can explain the Cu versus Au trend in the S-poor IVB group but not the decreasing Cu versus Au trends in the IIIAB and IIAB groups or the unique S-shaped IVA Cu versus Au trend. Debate exists about what S content is appropriate for each iron meteorite group, with crystallization models involving trapped melt by Wasson (1999), Wasson and Richardson (2001), and Wasson et al. (2007) advocating lower S contents than those suggested by the simple fractional crystallization models of Haack and Scott (1993), Ulff-Møller (1998), and Chabot (2004). However, in the case of Cu, the resulting Cu solid metal crystallization paths are relatively insensitive to the initial S content of the metallic liquid, as shown on Fig. 5b. Consequently, using different S contents for the iron meteorite groups does not result in better agreement between the simple fractional crystallization model trends and those of the IIAB, IIIAB, and IVA iron meteorite groups.

Sensitivity of the Model Results to the Choice of D(Cu)

Because the simple fractional crystallization model was unable to match the majority of Cu iron meteorite trends, we explored the effect of a small change in the expression of D(Cu) on the model results. For this exploration, we decided to use a simple linear fit to express D(Cu) as a function of the S content of the metallic liquid. The best-fit line is given by the equation:

$$D(Cu) = 0.57 - 0.015(wt\%S) \quad (8)$$

Figure 6a shows this linear fit and the D(Cu) experimental data. This linear "fit" does not provide as good of a match to the experimental D(Cu) data as the FeS domains based fit shown in Fig. 5a. This linear fit is also meaningless, as its functional form has no basis in understanding the influence of the metallic liquid on partitioning behavior, in contrast to the FeS domains based fit. Figure 6b shows the solid metal crystallization paths produced by using the linear fit to D(Cu) in the simple fractional crystallization model. For easy comparison, Fig. 6b is shown on the same scale as the plots in Fig. 5. Different initial bulk S contents produce different Cu versus Au concentration trends on Fig. 6b. Figure 6b shows that even though D(Cu) is less than unity, decreasing Cu versus Au trends can be produced by simple fractional crystallization. The decreasing trends are similar to those present in the IIIAB and IIAB iron meteorite groups seen on Figs. 5d and 5e. The decreasing trends arise because it is not just the value of D(Cu) that affects the resulting trends but also how D(Cu) changes during the crystallization process. It is a mathematical related rate problem involving the rate of change of the Cu concentration in the metallic liquid and the rate of change of D(Cu).

It is immediately clear by comparing Figs. 5b and 6b that the resulting crystallization trends using two different fits for D(Cu) are significantly different. This difference is unsettling. This exploration demonstrates that the fractional crystallization modeling of Cu is sensitive to the choice of the functional form for D(Cu). Our current best fit to D(Cu), based on our understanding of the influence of FeS domains in the metallic liquid, does not produce simple fractional crystallization Cu versus Au trends consistent with the IIAB, IIIAB, and IVA iron meteorite groups. However, the D(Cu) experimental data have scatter such that a slightly different D(Cu) fit would be permitted within the experimental uncertainties. This exploration work in Fig. 6 illustrates that slightly different parameterizations of D(Cu) have the potential to result in significantly different crystallization trends. Any refinement or improved understanding of D(Cu) in the future should thus also motivate a re-examination of Cu trends produced during fractional crystallization.

OTHER POTENTIAL INFLUENCES ON Cr AND Cu ABUNDANCES

Our crystallization modeling work indicates that neither the Cu nor Cr trends in magmatic iron meteorite groups, with the exception of the S-poor IVB group, are consistent with

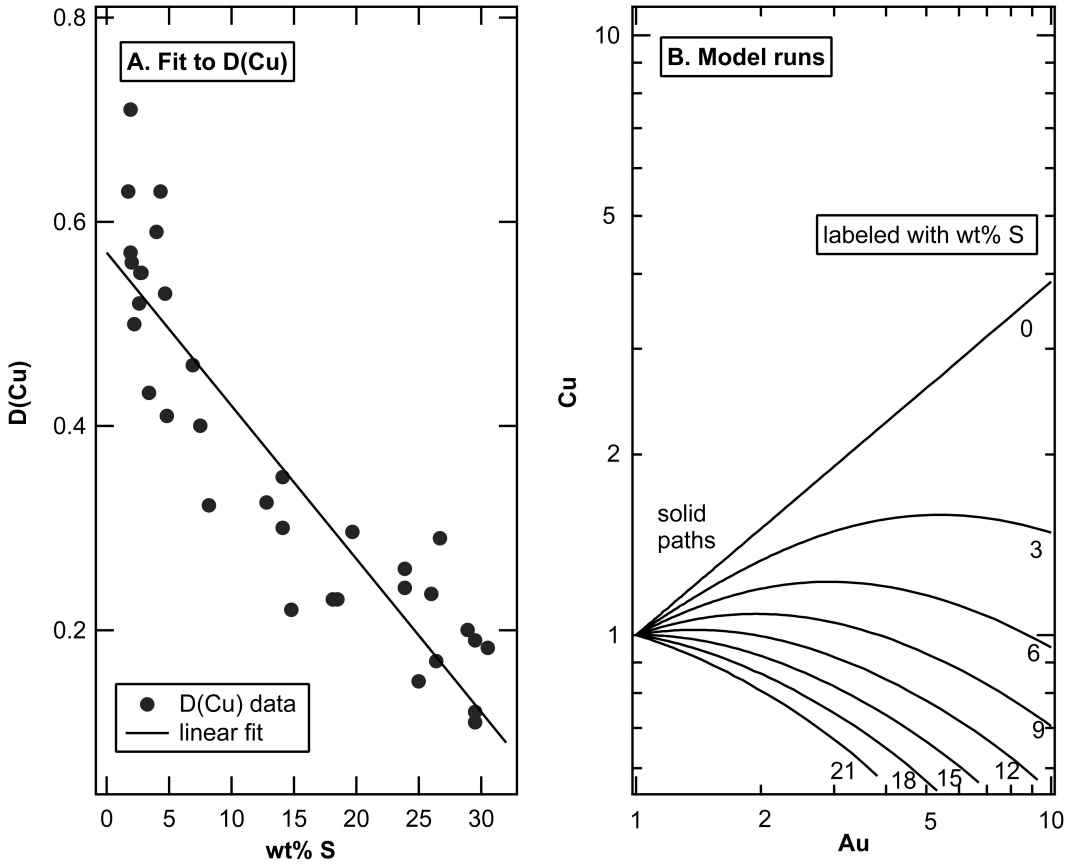

Fig. 6. A) A linear fit is shown to the D(Cu) experimental data. B) Using the linear fit, different Cu versus Au simple fractional crystallization trends are shown for different initial S contents. The model trends differ significantly from those shown in Fig. 5b, demonstrating that the choice of parameterization of D(Cu) has a significant effect on the model calculations.

being formed by simple fractional crystallization of solid metal. In the IIAB, IIIAB, and IVA iron meteorite groups, both the Cu/Ni and Cr/Ni ratios are significantly lower than those of CI chondrites (Palme and Jones 2005). This is in contrast to, for example, the Au/Ni ratios for these same three groups, which are similar to the CI chondrite Au/Ni ratio (Palme and Jones 2005). The IVB group has Cu/Ni, Cr/Ni, and Au/Ni ratios that are all much lower than those of CI chondrites. These depleted ratios indicate either that Cu and Cr were not segregated efficiently into the metallic melt during asteroid differentiation, that Cu and Cr were concentrated in phases other than the solid metal during crystallization of these iron meteorite groups, that these iron meteorite parent bodies had bulk starting compositions significantly different than CI chondrites, or that a combination of these effects occurred. If the parent body bulk composition or the lithophile tendencies of Cr and Cu resulted in the segregated metallic melt being depleted in these elements relative to Ni, the resulting crystallization trends would still have the same shape but just a lower absolute abundance of Cr and Cu. Since our simple fractional crystallization modeling is unable to reproduce the decreasing nature of the IIAB, IIIAB, and IVA Cu versus Au trends and any of the steeply negative Cr versus Au trends, some additional effect operating during and/or after the crystallization of these iron meteorite groups must have had an influence on the resulting trends of these elements.

Wasson et al. (1999) listed four options for explaining the decreasing Cr versus Au trend in the IIIAB iron meteorite group:

1. Cr is compatible during crystallization and the experimental D(Cr) values are incorrect.
2. Cr is extracted from the melt during crystallization by another phase, such as chromite ($FeCr_2O_4$).
3. D(Cr) is <1 but decreases with increasing S content of the metallic liquid at such a rate as to more than compensate for the increasing Cr content in the melt.
4. The apparent Cr trend is a sampling artifact, due to bulk analyses of iron meteorites avoiding large chromite grains.

Wasson et al. (1999) quickly dismissed option 1, and our new experimental data for D(Cu) and D(Cr), plotted in Fig. 4, further confirm the incompatible behavior for these elements during fractional crystallization in the Fe-Ni-S system. Our new experimental data also rule out option 3, which Wasson et al. (1999) concluded was unlikely, but lacked the necessary

partitioning data at the time to fully evaluate. Our experimental results indicate that both D(Cu) and D(Cr) decrease with increasing S content of the metallic liquid but our modeling results quantitatively show that the decrease in D(Cu) (and D(Cr) by its similarity) is not drastic enough to result in decreasing fractional crystallization trends as observed in the iron meteorite groups.

Wasson et al. (1999) ultimately concluded that the decreasing Cr versus Au trend in the IIIAB iron meteorite group was most likely the result of option 4, a sampling artifact introduced during the analytical measurements. This is consistent with decreasing Cr content resulting from analysts avoiding visible inclusions when selecting iron meteorites for compositional measurements and Cr diffusing out of the solid metal and into large chromite grains in the iron meteorites. Buchwald (1975) documents large chromite grains found in iron meteorites, some many centimeters in size. Wasson et al. (1999) cited the high amount of scatter in Cr measurements for high-Au, later crystallizing irons, including some evolved irons with high Cr contents, as evidence that Cr was being redistributed in these irons subsequent to crystallization. They argued that removing a Cr-rich phase, such as chromite, during crystallization would not explain the large amount of scatter observed in the iron meteorite Cr trends.

There is no doubt that large chromite inclusions are avoided during bulk compositional measurements of iron meteorites, and Wasson et al. (2007) when studying the IIAB iron meteorite group suggested that both sampling biases and the formation of chromite during crystallization may contribute to the Cr trends seen in Fig. 1. Due to the density differences, chromite would rise and separate from the metallic melt. This flotation fractionation of chromite and its removal from the crystallizing system could make Cr appear to be compatible during the crystallization of asteroidal cores, producing decreasing Cr versus Au trends in iron meteorite groups. Chromite, along with carlsbergite (CrN) and daubreelite ($FeCr_2S_4$), are phases commonly identified in iron meteorites (Buchwald 1975). If flotation fractionation of chromite and its removal from the crystallizing system did occur, it could have implications for understanding the direction of crystallization of an asteroidal core. It would be easier to remove a chromite phase that floats if the core crystallized from the center outwards, while crystallization from the core-mantle boundary inward would make it difficult for chromite to escape the crystallizing system.

Based on this idea of chromite removal during iron meteorite crystallization, we predict that V, too, should appear to behave compatibly in iron meteorites, even though it behaves incompatibly in our experiments. Vanadium partitions strongly into chromite in silicate systems; its behavior in metallic systems is relatively unknown, though Wasson et al. (1999) reported V concentrations in chromites from four IIIAB irons. Also, it is probable that the composition of minor-elements in iron meteorite chromites is mainly determined by subsolidus equilibration, not magmatic partitioning. Still, V is fundamentally a lithophile element and we predict that, when presented with the opportunity, it will strongly partition into an oxide phase. Data on IVB metals from both Campbell and Humayun (2005) and Walker et al. (2008) show that the IVB V versus Au trend decreases steeply, similar to the IVB Cr versus Au trend. Though the decreasing Cr and V versus Au trends in IVB irons could be due to site selection effects during the analytical procedure, the high Ni content of IVB irons makes them ataxites and therefore highly homogeneous on the scale of the analyses. The removal of chromite during crystallization could explain both the decreasing Cr and V versus Au trends in the IVB group. Measuring V in chromites from irons that span the range of compositions found in iron meteorite groups could also provide insight into the presence of chromite during iron meteorite crystallization. To our knowledge, a complete study of chromite compositions such as this has not been attempted.

The Cu iron meteorite trends decrease less steeply than those of Cr, as shown in Fig. 1. However, our simple fractional crystallization model does not produce any decreasing Cu trends, as shown in Fig. 5. The removal of chromite during crystallization does not seem able to explain the decreasing iron meteorite Cu trends, and, as discussed previously, Wasson and Richardson (2001) state that sampling artifacts did not influence the iron meteorite Cu measurements. The sensitivity of our fractional crystallization modeling to the choice of D(Cu) leaves open the small possibility that the decreasing Cu trends may yet be fit by fractional crystallization with a future refinement to the parameterization of D(Cu). Otherwise, the decreasing Cu trends in the IIAB and IIIAB groups and the unique S-shaped Cu trend in the IVA group require an explanation.

SUMMARY

We report new solid metal/liquid metal experimental partition coefficients for 15 elements over a range of S contents in the Fe-Ni-S system. Nine of the elements exhibited classic siderophile behavior, with increasing D values as the S content of the metallic liquid increased: As, Au, Co, Mo, Ni, Rh, Ru, Sb, and Sn. In contrast, five of the investigated trace elements exhibited chalcophile behavior, showing decreasing D values with increasing S contents: Bi, Pb, Cr, Cu, and V. The partitioning behavior of Zn was determined to be unique among the elements in our study, with a constant D value despite changing S concentrations in the metallic melt. Our new partitioning results are in good agreement with the previously available experimental determinations.

Over the full range of S contents in the Fe-Ni-S system Cu and Cr have very similar solid metal/liquid metal partitioning values. However, very different trends for Cu and Cr versus Au are found for iron meteorite groups. Thus, Cu and Cr versus Au trends within these iron meteorite groups cannot both be formed by fractional crystallization.

Simple fractional crystallization calculations were performed and compared to iron meteorite Cu versus Au trends using a FeS domains based fit for D(Cu). The Cu versus Au trend in the S-poor IVB group is consistent with being formed by simple fractional crystallization. The decreasing Cu versus Au trends in the IIAB and IIIAB groups and the distinctive S-shaped IVA Cu versus Au trend were not reproduce by our simple fractional crystallization model. However, our modeling work demonstrates that the fractional crystallization model calculations are sensitive to the specific choice of the parameterization of D(Cu). Any future refinement of the mathematical parameterization of D(Cu) should thus motivate a re-examination of the Cu trends produced during fractional crystallization.

Trends for Cr versus Au in the IIAB, IIIAB, IVA, and IVB meteorite groups show larger decreases than the Cu versus Au trends, and our work suggests that the Cr versus Au trends observed in these groups are not produced solely by fractional crystallization. Additional influences, such as the formation of chromite during crystallization or sampling artifacts during iron meteorite compositional analyses, were likely involved in creating the observed Cr concentrations in magmatic iron meteorites. If the formation and removal of chromite did occur during crystallization, it could have implications for understanding the direction of growth (outward from the center versus inward for the core-mantle boundary) of asteroidal cores.

Acknowledgments—We thank reviewers A. Kracher and H. Haack and associate editor E. R. D. Scott for constructive and thoughtful comments that resulted in substantial improvements to this paper. We also thank Y. Fei of the Geophysical Laboratory at the Carnegie Institution of Washington for supporting this study by providing access to the JEOL 8900L electron microprobe. This work was supported by NASA grant NNG06GI13G to NLC and NNX08AH76G to WFM and a NASA RTOP to JHJ.

Editorial Handling—Dr. Edward Scott

REFERENCES

Achterbergh E. V., Ryan C. G., Jackson S. E., and Griffin W. L. 2001. Appendix 3: Data reduction software for LA-ICP-MS. In *Laser ablation-ICP-MS in the earth sciences*, vol. 29, edited by Sylvester P. Mineralogical Association of Canada, Short Course Series. 243 p.

Bild R. W. and Drake M. J. 1978. Experimental investigations of trace element fractionation in iron meteorites. I—Early results. Proceedings, 9th Lunar and Planetary Science Conference. pp. 1407–1421.

Buchwald V. F. 1975. *Handbook of iron meteorites*. Berkeley: University of California Press. 1418 p.

Campbell A. J. and Humayun M. 2005. Composition of group IVB iron meteorites and their parent melt. *Geochimica et Cosmochimica Acta* 69:4733–4744.

Chabot N. L. 2004. Sulfur contents of the parental metallic cores of magmatic iron meteorites. *Geochimica et Cosmochimica Acta* 68:3607–3618.

Chabot N. L. and Agee C. B. 2003. Core formation in the Earth and Moon: New experimental constraints from V, Cr, and Mn. *Geochimica et Cosmochimica Acta* 67:2077–2091.

Chabot N. L. and Drake M. J. 1997. An experimental study of silver and palladium partitioning between solid and liquid metal, with applications to iron meteorites. *Meteoritics & Planetary Science* 32:637–645.

Chabot N. L. and Haack H. 2006. Evolution of asteroidal cores. In *Meteorites and the early solar system II*, edited by Lauretta D. S. and McSween Jr. H. Y. Tucson: The University of Arizona Press. pp. 747–771.

Chabot N. L. and Jones J. H. 2003. The parameterization of solid metal-liquid metal partitioning of siderophile elements. *Meteoritics & Planetary Science* 38:1425–1436.

Chabot N. L., Campbell A. J., Jones J. H., Humayun M., and Agee C. B. 2003. An experimental test of Henry's Law in solid metal-liquid metal systems with implications for iron meteorites. *Meteoritics & Planetary Science* 38:181–196.

Chabot N. L., Saslow S. A., McDonough W. F., and McCoy T. J. 2007. The effect of Ni on element partitioning during iron meteorite crystallization. *Meteoritics & Planetary Science* 42: 1735–1750.

Corrigan C. M., Chabot N. L., McCoy T. J., McDonough W. F., Watson H. C., Saslow S. A., and Ash R. D. 2009. The iron-nickel-phosphorus system: Effects on the distribution of trace elements during the evolution of iron meteorites. *Geochimica et Cosmochimica Acta* 73:2674–2691.

Fleet M. E. and Stone W. E. 1991. Partitioning of platinum-group elements in the Fe-Ni-S system and their fractionation in nature. *Geochimica et Cosmochimica Acta* 55:245–253.

Fleet M. E., Liu M., and Crocket J. H. 1999. Partitioning of trace amounts of highly siderophile elements in the Fe-Ni-S system and their fractionation in nature. *Geochimica et Cosmochimica Acta* 63:2611–2622.

Haack H. and Scott E. R. D. 1993. Chemical fractionations in group IIIAB iron meteorites: Origin by dendritic crystallization of an asteroidal core. *Geochimica et Cosmochimica Acta* 57:3457–3472.

Hongsresawat S., Chabot N. L., and Jones J. H. 2002. Modeling the solidification of magmatic iron meteorites using experimental Cu partitioning (abstract #1337). 33rd Lunar and Planetary Science Conference. CD-ROM.

Jones J. H. 1994. Fractional crystallization of iron meteorites: Constant versus changing partition coefficients. *Meteoritics* 29: 423–426.

Jones J. H. and Drake M. J. 1983. Experimental investigations of trace element fractionation in iron meteorites, II: The influence of sulfur. *Geochimica et Cosmochimica Acta* 47:1199–1209.

Jones J. H. and Drake M. J. 1986. Geochemical constraints on core formation in the Earth. *Nature* 322:221–228.

Jones J. H. and Malvin D. J. 1990. A nonmetal interaction model for the segregation of trace metals during solidification of Fe-Ni-S, Fe-Ni-P, and Fe-Ni-S-P alloys. *Metallurgical and Materials Transactions B* 21:697–706.

Jones J. H., Hart S. R., and Benjamin T. M. 1993. Experimental partitioning studies near the Fe-FeS eutectic, with an emphasis on elements important to iron meteorite chronologies (Pb, Ag, Pd, and Tl). *Geochimica et Cosmochimica Acta* 57:453–460.

Liu M. and Fleet M. E. 2001. Partitioning of siderophile elements (W, Mo, As, Ag, Ge, Ga, and Sn) and Si in the Fe-S system and their fractionation in iron meteorites. *Geochimica et Cosmochimica Acta* 65:671–682.

Lodders K. and Palme H. 1991. On the chalcophile character of molybdenum: Determination of sulfide/silicate partition coefficients of Mo and W. *Earth and Planetary Science Letters* 103:311–324.

Malvin D. J., Jones J. H., and Drake M. J. 1986. Experimental

investigations of trace element fractionation in iron meteorites. III: Elemental partitioning in the system Fe-Ni-S-P. *Geochimica et Cosmochimica Acta* 50:1221–1231.

Palme H. and Jones A. 2005. Solar system abundances of the elements. In *Meteorites, comets, and planets*, edited by Davis A. M. Treatise on Geochemistry, vol. 1. Oxford: Elsevier. pp. 41–61.

Scott E. R. D. 1972. Chemical fractionation in iron meteorites and its interpretation. *Geochimica et Cosmochimica Acta* 36:1205–1236.

Ulff-Møller F. 1998. Effects of liquid immiscibility on trace element fractionation in magmatic iron meteorites: A case study of group IIIAB. *Meteoritics & Planetary Science* 33: 207–220.

Walker R. J., McDonough W. F., Honesto J., and Chabot N. L. 2008. Modeling fractional crystallization of group IVB iron meteorites. *Geochimica et Cosmochimica Acta* 72:2198–2216.

Wasson J. T. 1999. Trapped melt in IIIAB irons; solid/liquid elemental partitioning during the fractionation of the IIIAB magma. *Geochimica et Cosmochimica Acta* 63:2875–2889.

Wasson J. T. and Richardson J. W. 2001. Fractionation trends among IVA iron meteorites: Contrasts with IIIAB trends. *Geochimica et Cosmochimica Acta* 65:951–970.

Wasson J. T., Choi B.-G., Jerde E. A., and Ulff-Møller F. 1998. Chemical classification of iron meteorites: XII. New members of the magmatic groups. *Geochimica et Cosmochimica Acta* 63: 2875–2889.

Wasson J. T., Lange D. E., Francis C. A., and Ulff-Møller F. 1999. Massive chromite in the Brenham pallasite and the fractionation of Cr during the crystallization of asteroidal cores. *Geochimica et Cosmochimica Acta* 63:1219–1232.

Wasson J. T., Huber H., and Malvin D. J. 2007. Formation of the IIAB iron meteorites. *Geochimica et Cosmochimica Acta* 71:760–781.

Willis J. and Goldstein J. I. 1982. The effects of C, P, and S on trace element partitioning during solidification in Fe-Ni alloys. Proceedings, 13th Lunar and Planetary Science Conference, Part I. *Journal of Geophysical Research* 87:A435–A445.

APPENDIX A

References are given in Table A1 for previous experimental determinations of solid metal/liquid metal partition coefficients in the Fe-Ni-S system, for Ni contents <20 wt%.

Table A1. References for previous experimental solid metal/liquid metal partitioning data and number of partition coefficients per element from each study.

Reference	As	Au	Co	Cr	Cu	Mo	Ni	Rh	Ru	Sb	Sn
Appendix B					11		11				
Bild and Drake (1978)		1	1	1			4				
Chabot et al. (2003)	21		11	3	17		42			3	
Fleet and Stone (1991)							5	9			
Fleet et al. (1999)		2					4		2		
Jones et al. (1993)		1				1					
Jones and Drake (1983)		9	1			1	28				
Jones and Malvin (1990)		5	3	1			15				
Liu and Fleet (2001)	6					4					7
Lodders and Palme (1991)						1					
Willis and Goldstein (1982)							5				

APPENDIX B

Hongsresawat et al. (2002) presented preliminary results for Cu and Ni partitioning in the Fe-Ni-S-Cr system at the Lunar and Planetary Science Conference. Table B1 provides final compositions and partitioning results from that study.

Table B1. Experimental compositions and partitioning results.

Run name	Eta	Epsilon	Alpha	Cr1	Beta	Gamma	Zeta 1	Zeta 2	Zeta 3	Zeta 4	Theta
T (°C)	1015	1150	1250	1325	1340	1350	1385	1385	1385	1385	1420
Time (days)	6	5	4	3	2	2	1	1	1	1	1
Solid metal											
Fe	82.0 ± 0.7	86.1 ± 0.7	87.0 ± 0.5	89.4 ± 0.4	89.7 ± 0.6	89.9 ± 0.4	90.0 ± 1.0	89.9 ± 0.7	88.8 ± 0.8	90.1 ± 0.4	90.2 ± 0.5
Ni	17.3 ± 0.7	13.4 ± 0.3	13.1 ± 0.1	10.5 ± 0.1	10.4 ± 0.1	10.3 ± 0.1	9.2 ± 0.2	10.3 ± 0.2	9.9 ± 0.3	10.2 ± 0.1	10.0 ± 0.2
Cu	0.13 ± 0.07	0.19 ± 0.1	0.21 ± 0.04	0.54 ± 0.04	0.31 ± 0.04	0.27 ± 0.04	0.33 ± 0.08	0.38 ± 0.04	0.32 ± 0.09	0.40 ± 0.03	0.32 ± 0.04
Total	99.4	99.7	100.3	100.4	100.4	100.5	99.5	100.6	99.0	100.7	100.5
Liq. metal											
Fe	59.2 ± 0.8	61.7 ± 1.5	65.2 ± 2.7	70.1 ± 2.0	75.1 ± 2.0	75.4 ± 2.3	81.8 ± 1.3	84.7 ± 1.2	81.4 ± 1.5	83.8 ± 1.2	84.9 ± 0.8
Ni	8.9 ± 0.7	9.3 ± 0.7	9.7 ± 0.9	9.4 ± 0.6	10.2 ± 0.6	10.0 ± 0.6	9.8 ± 0.2	11.0 ± 0.2	10.8 ± 0.2	11.0 ± 0.2	10.8 ± 0.8
S	29.5 ± 1.1	26.7 ± 1.6	23.9 ± 3.1	18.1 ± 1.8	14.1 ± 2.2	14.1 ± 2.5	6.9 ± 1.3	4.3 ± 1.1	7.5 ± 1.4	4.7 ± 1.0	4.0 ± 0.8
Cu	0.70 ± 0.08	0.66 ± 0.10	0.80 ± 0.14	2.4 ± 0.4	0.89 ± 0.12	0.90 ± 0.16	0.72 ± 0.09	0.60 ± 0.05	0.80 ± 0.10	0.76 ± 0.10	0.54 ± 0.05
Total	98.3	98.4	99.6	100.0	100.3	100.4	99.2	100.6	100.5	100.3	100.2
D(Ni)	1.9 ± 0.2	1.44 ± 0.11	1.35 ± 0.13	1.12 ± 0.07	1.02 ± 0.06	1.03 ± 0.06	0.94 ± 0.03	0.94 ± 0.02	0.92 ± 0.03	0.93 ± 0.02	0.93 ± 0.07
D(Cu)	0.19 ± 0.10	0.29 ± 0.16	0.26 ± 0.07	0.23 ± 0.04	0.35 ± 0.07	0.30 ± 0.07	0.46 ± 0.13	0.63 ± 0.09	0.40 ± 0.12	0.53 ± 0.08	0.59 ± 0.09

All measurements are reported as wt%. Errors are 2σ.